

Toward the Development of Measurement Integrated Simulation

Hiroshi Kato
Shigeru Obayashi

Institute of Fluid Science
Tohoku University
Sendai, 980-8577
Japan
kato@edge.ifs.tohoku.ac.jp

Abstract

In this research, the ensemble Kalman filter, a data assimilation method, is employed to estimate the turbulent viscosity for the flow field around the RAE2822 airfoil. The turbulent viscosity is estimated directly from the experimental pressure distribution on the airfoil, without a turbulence model. The turbulent viscosity estimated by the ensemble Kalman filter shows lower magnitude around the airfoil than that estimated with the Spalart–Allmaras turbulence model and is almost zero in the wake region. Computation with the estimated turbulent viscosity can predict the separated flow region at the shock-boundary layer interaction. Due to this separation, the computed pressure coefficient agrees better with the experiment. These results suggest that this data assimilation method can be used to estimate the turbulent viscosity without a turbulence model.

Key words: EFD/CFD, measurement integrated simulation, data assimilation, turbulence model

Introduction

Wind tunnel experiments (EFD: Experimental Fluid Dynamics) and numerical simulation (CFD: Computational Fluid Dynamics) have been used to predict the aerodynamic characteristics of aircraft and spacecraft. With the remarkable development of CFD techniques, methods for the integration of EFD and CFD (EFD/CFD, which our group calls EFD/CFD “measurement integrated simulation”) have been discussed for prediction of aerodynamic characteristics with higher accuracy, efficiency, and reliability than either EFD or CFD alone [1].

To achieve EFD/CFD, the meaning of the word “integration” should first be defined. The definition of the word “integration” differs between groups, which results in the various realization of EFD/CFD. Various methods to integrate EFD and CFD are available.

Currently, the authors are focusing on turbulent viscosity—a method to represent the Reynolds stress term in the Reynolds-averaged Navier–Stokes (RANS) equations—to integrate EFD and CFD. Turbulent viscosity is computed by a turbulence model, such as the Spalart–Allmaras model [2] or the Menter SST model [3]. The computation is strongly affected by turbulent viscosity; however, most turbulence models still cannot be used for precise analysis of complex flows. Obviously, the large eddy simulation (LES) and direct numerical simulation (DNS) can be used to accurately compute fluid phenomena, because the equations employed in LES and DNS have fewer approximations than that of RANS. However, LES and DNS are not yet practical tools to predict aerodynamic characteristics efficiently, as they require massive computational resources and time. In the engineering field, CFD is expected to be an efficient tool for prediction of aerodynamic characteristics. Therefore, RANS simulation is essential as a design tool, and a method to compute the turbulent viscosity with a high accuracy will be required in future.

In the field of engineering, turbulence models are techniques to represent the turbulent viscosity. Turbulence models include artificial parameters unlike the Navier–Stokes equations, and actually different turbulence models yield different results for complex flows.

In the past, our group adjusted the parameter values in the Spalart–Allmaras turbulence model using experimentally obtained values for more precise computation than that with CFD alone [4, 5, 6]. Our previous studies showed the following:

1. Different turbulence models can predict the same flow field by adjusting the parameter values in a turbulence model.
2. The parameter values calibrated by the model proposer, Spalart and Allmaras, are determined by the ensemble Kalman filter.
3. Computation with the adjusted parameter values agrees with the experimental values better than that with the original parameter values.

These results suggest that computation integrating a turbulence model with experimental results can predict fluid phenomena better than CFD alone. On the other hand, the method to adjust the parameter values in the turbulence model was able to not compute the turbulent viscosity beyond the solution space of the turbulence model; that is, even computation integrating a turbulence model with experiment cannot predict fluid phenomena with the turbulent viscosity that current turbulence models cannot express.

This study was performed to investigate computation of the turbulent viscosity directly from experimental values without a turbulence model. For the investigation, the flow field around the RAE2822 airfoil [7] was computed. The method can compute the turbulent viscosity beyond the solution space of the turbulence model; that is, the computation with experimental values can predict fluid phenomena with the turbulent viscosity that current turbulence models cannot express. The ensemble Kalman filter [8], a data assimilation method [9], can be applied to compute the turbulent viscosity from experimental values.

The rest of the paper is organized as follows. The methods are described in Section 2. Section 3 describes the procedure of the ensemble Kalman filter. Section 4 describes the results. Finally, the conclusion is presented in Section 5.

Methods

I. Ensemble Kalman filter

The ensemble Kalman filter (EnKF) is a data assimilation method. Data assimilation was developed as a method combining observation (experiment) and numerical simulation in the field of meteorological and oceanic research. Data assimilation methods can estimate the optimal state variables for nonlinear and large-scale systems, such as flow simulation.

The nonlinear system can be expressed as in Eq. (1).

$$\mathbf{x}_t = \mathbf{f}_t(\mathbf{x}_{t-1}), \quad (1)$$

where \mathbf{x}_t represents the state variables. In the Reynolds-averaged Navier–Stokes (RANS) simulation with turbulent viscosity $\boldsymbol{\mu}_t$, \mathbf{x}_t consists of the state variables as shown in Eq. (2).

$$\mathbf{x}_t = (\boldsymbol{\rho}, \mathbf{u}, \mathbf{v}, \mathbf{w}, \mathbf{p}, \boldsymbol{\mu}_t)^T, \quad (2)$$

where $\boldsymbol{\rho}$ represents the density, $\mathbf{u}, \mathbf{v}, \mathbf{w}$ represent the velocity components, and \mathbf{p} represents the pressure. Generally, the density, the velocity components, and the pressure are calculated from the RANS equations, and the turbulent viscosity is calculated from an additional model that is called the “turbulence model.”

The ensemble Kalman filter estimates the optimal state variables through the following procedure:

1. Determine the initial ensemble members $\{\mathbf{x}_0^{(i)}\}_{i=1}^N$ and $t \leftarrow 1$.
2. At time t
(Prediction step)

- A) Generate system noise $\{\mathbf{v}_t^{(i)}\}_{i=1}^N$. (System noise was not considered in this study)
- B) Calculate $\mathbf{x}_t^{(i)} = f_t(\mathbf{x}_{t-1}^{(i)}, \mathbf{v}_t^{(i)})$ for each ensemble member.
(Filtering step)
- A) Generate observation noise $\{\mathbf{w}_t^{(i)}\}_{i=1}^N$.
- B) Calculate variance-covariance matrix $\hat{\mathbf{V}}_t$, $\hat{\mathbf{R}}_t$, and Kalman gain $\hat{\mathbf{K}}_t$.
- C) Calculate $\mathbf{x}_t^{(i)} = \mathbf{x}_t^{(i)} + \hat{\mathbf{K}}_t(\mathbf{y}_t - \mathbf{H}_t\mathbf{x}_t^{(i)} + \mathbf{w}_t^{(i)})$ for each ensemble member.
3. Set $t \leftarrow t + 1$ and repeat step 2.

In the above procedure, $\{\mathbf{x}_t^{(i)}\}_{i=1}^N$ is the ensemble of $\mathbf{x}_t^{(i)}$, \mathbf{y}_t represents the experimental values, and N is the number of realizations, which is called the “ensemble number.”

The detailed procedure of the ensemble Kalman filter is presented in the next section. (For the detailed mathematical description of the ensemble Kalman filter, please refer to [10, 11, 12], etc.)

II. Computational schemes

In this study, the fast aerodynamic routine (FaSTAR) [13] developed by the Japan Aerospace Exploration Agency (JAXA) was used for flow simulation. FaSTAR has several computational schemes, and we used those shown in Table 1.

Table 1. Computational schemes used in this study

| | Schemes |
|------------------|-------------------------------------------|
| Inviscid flux | HLLEW |
| Gradient Limiter | Least-square Van Leer original limiter |
| Viscous flux | Cell gradient |
| Time integration | LU-SGS |

III. Calculation conditions

The calculation conditions were: Mach number, 0.729; Reynolds number, 6.5×10^6 ; and angle of attack, 2.31. RANS computation was performed with CFL number of about 1200, and 5 inner iterations.

IV. Computational grid

The computational grid with a minimum grid spacing of 3.9×10^{-6} , where the chord length of the RAE 2822 airfoil was set to 1 as the reference length, was prepared. Figure 1 shows the computational grid. Reference [6] showed that the grid resolution was sufficient for the computation.

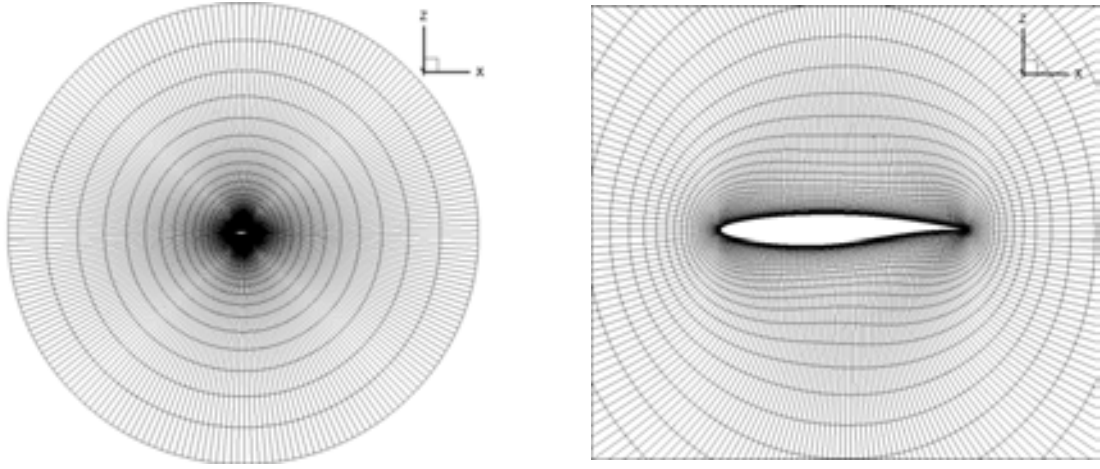


Figure 1. Computational grid

V. Experimental values

The ensemble Kalman filter requires experimental values to estimate the optimal state variables. The pressure coefficient data from a wind tunnel experiment corresponding to the calculation conditions have been released on the NASA website in the file cp.exp.gen [14]. The non-dimensional pressure data were calculated from the pressure coefficient data using Eq. (3), a non-dimensional formula for the pressure coefficient. The data were utilized as experimental values \mathbf{y}_t for the EnKF.

$$C_p = \frac{\left(p - \frac{1}{\gamma}\right)}{\frac{1}{2}M^2}, \quad (3)$$

where C_p is the pressure coefficient, γ is the specific heat ratio of 1.4, and M is the Mach number of 0.729.

Procedure

I. Prediction step

The ensemble Kalman filter requires different state variables in each ensemble member at the beginning of the filtering step. For this requirement, various methods are available, such as assigning different boundary conditions or different initial conditions to each ensemble member. In this study, the state variables of each ensemble member were first computed with the Spalart–Allmaras turbulence model using the different parameter values for each ensemble member. As the parameter values were different for each ensemble member, each computed state variable was different. Then, the different state variables were assigned to each ensemble member. The Spalart–Allmaras turbulence model was used only for the assignment.

The values of each parameter of the Spalart–Allmaras turbulence model were selected equally from the ranges as in Eqs. (4)–(8) using Latin hypercube sampling [15]. Each range was defined by half of the original value of each parameter. Superscript (l) in Eqs. (4)–(8) indicates the number of the ensemble member.

$$5.325 < C_{v1}^{(l)} < 8.875 \quad (4)$$

$$0.101625 < C_{b1}^{(l)} < 0.169375 \quad (5)$$

$$0.4665 < C_{b2}^{(l)} < 0.7775 \quad (6)$$

$$0.225 < C_{\omega 2}^{(l)} < 0.375 \quad (7)$$

$$1.5 < C_{\omega 3}^{(l)} < 2.5 \quad (8)$$

II. Filtering step

The prediction step was repeated in each ensemble member to 50000 time steps to converge the computation in each ensemble member. Then, the filtering step was performed every 2000 prediction steps until 80000 time steps. The filtering step was performed through the following 6 steps. The number 100 in the equations below indicates the number of ensemble members in this study.

- 1) Calculate ensemble mean $\bar{\mathbf{x}}_t^*$

$$\bar{\mathbf{x}}_t^* = \frac{1}{100} \sum_{l=1}^{100} \mathbf{x}_t^{*(l)} \quad (9)$$

- 2) Calculate variance-covariance matrix $\bar{\mathbf{V}}_t$

$$\bar{\mathbf{V}}_t = \frac{1}{100 - 1} \sum_{l=1}^{100} (\mathbf{x}_t^{*(l)} - \bar{\mathbf{x}}_t^*)(\mathbf{x}_t^{*(l)} - \bar{\mathbf{x}}_t^*)^T \quad (10)$$

- 3) Generate experimental noise \mathbf{w}_t

$$\mathbf{w}_t^{(l)} = N(\mathbf{0}, 1.0 \times 10^{-6} \mathbf{I}) \quad (11)$$

\mathbf{I} in (11) represents the unit matrix.

- 4) Calculate variance-covariance matrix of experimental noise $\bar{\mathbf{R}}_t$

$$\bar{\mathbf{R}}_t = \frac{1}{100 - 1} \sum_{l=1}^{100} \mathbf{w}_t^{(l)} \mathbf{w}_t^{(l)T} \quad (12)$$

- 5) Calculate Kalman gain $\bar{\mathbf{K}}_t$

$$\bar{\mathbf{K}}_t = \bar{\mathbf{V}}_t \mathbf{H}_t (\bar{\mathbf{R}}_t + \mathbf{H}_t \bar{\mathbf{V}}_t \mathbf{H}_t^T)^{-1} \quad (13)$$

Superscript -1 in Eq. (13) shows the inverse matrix. \mathbf{H}_t represents the observation matrix used to extract experimental values from state variables.

- 6) Kalman filtering

$$\mathbf{x}_t^{*(l)} = \mathbf{x}_t^{*(l)} + \bar{\mathbf{K}}_t (\mathbf{y}_t - \mathbf{H}_t \mathbf{x}_t^{*(l)} + \mathbf{w}_t^{(l)}) \quad (14)$$

In the Kalman filtering step, when the filtered turbulent viscosity was less than 0, the turbulent viscosity was set to 0. This process was required to avoid divergence of the computation.

III. Re-computation

The ensemble Kalman filter estimated the optimal state variables—density, velocity components, pressure, and turbulent viscosity—based on the experimental values. Then, the density, the velocity components, and the pressure were re-computed using the computational schemes alone so that the state variables other than the turbulent viscosity satisfied the computational schemes. This re-computation is not strictly necessary for data assimilation, but researchers of numerical simulation have questioned whether the state variables estimated by

the ensemble Kalman filter satisfy the computational schemes. Therefore, the state variables other than the turbulent viscosity were re-computed using the computational schemes alone to avoid such questions. The density, velocity components, and pressure estimated by the ensemble Kalman filter were used for the initial conditions of re-computation, and the estimated turbulent viscosity was fixed during re-computation.

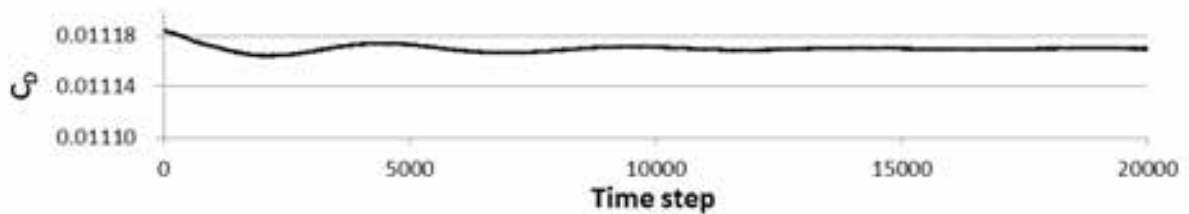
Results

This section discusses a comparison of computation with the SA-R model using the original parameter values (SA-R model), that with the SA-R model using the adjusted parameter values in reference [6] (Parameter value estimation), and that with the turbulent viscosity estimated by the ensemble Kalman filter (Turbulent viscosity estimation).

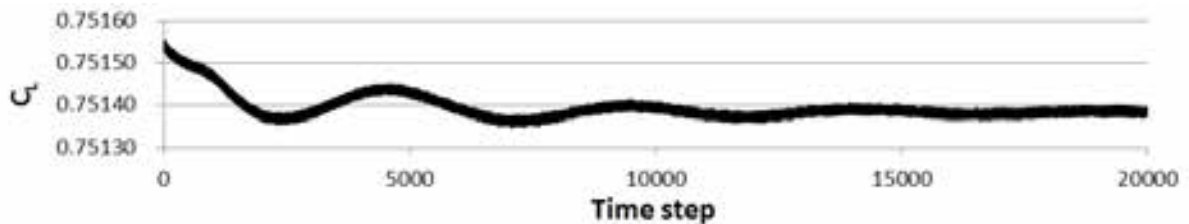
First, the re-computation histories for the density residual, the drag coefficient (C_D), the lift coefficient (C_L), and the moment coefficient (C_m) at 25% of the chord length are shown in Fig. 2. These figures show that the computation gradually converged to 20000 time steps.



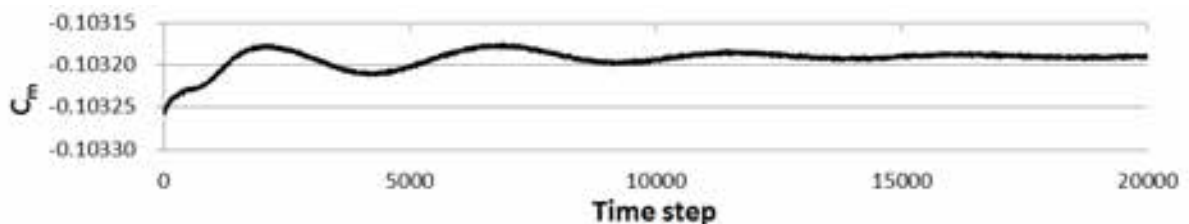
(a) Density residual



(b) Drag coefficient (C_D)



(c) Lift coefficient (C_L)



(d) Moment coefficient (C_m)

Figure 2. Re-computation history

Next, the computed pressure coefficients on the airfoil of each are compared with the experimental values in Fig. 3 and Fig. 4. In Fig. 3 and Fig. 4, the blue point shows the experimental pressure coefficient, the black dotted line shows the computed pressure coefficient with the turbulent viscosity of the SA-R model using the original parameter values (SA-R model), the green line shows that with the turbulent viscosity of the SA-R model using the adjusted parameter values (Parameter value estimation), and the red line shows that with the turbulent viscosity of the ensemble Kalman filter (Turbulent viscosity estimation).

The comparison shows that:

1. On the upper surface, the computed pressure coefficient of “Parameter value estimation” and “Turbulent viscosity estimation” agrees with the experimental pressure coefficient better than that of “SA-R model.”
2. At the shock-boundary layer interaction, the computed pressure coefficient of “Turbulent viscosity estimation” agrees with the experimental pressure coefficient better than those of “SA-R model” and “Parameter value estimation.”
3. At the trailing edge, the computed pressure coefficient of “Parameter value estimation” and “Turbulent viscosity estimation” agrees with the experimental pressure coefficient better than that of “SA-R model.”

These observations indicate that computation with “Turbulent viscosity estimation” can predict the proper fluid phenomena. Actually, at the shock-boundary layer interaction, the computed pressure coefficient with “Turbulent viscosity estimation” agreed well with the experimental pressure coefficients. This result suggests that the ensemble Kalman filter can be used to estimate the proper turbulent viscosity based on the experimental values.

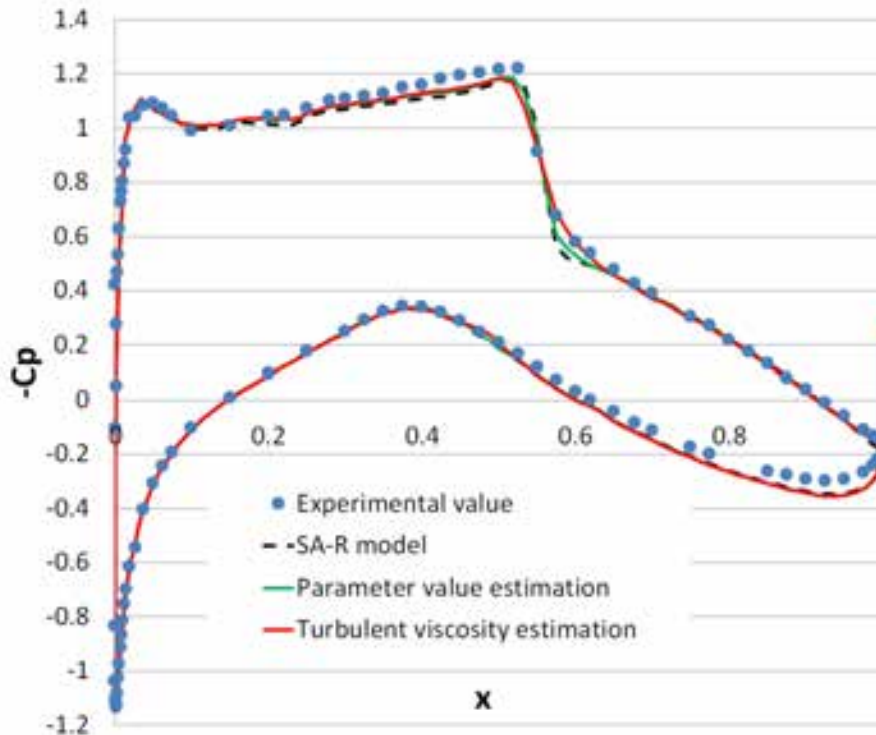
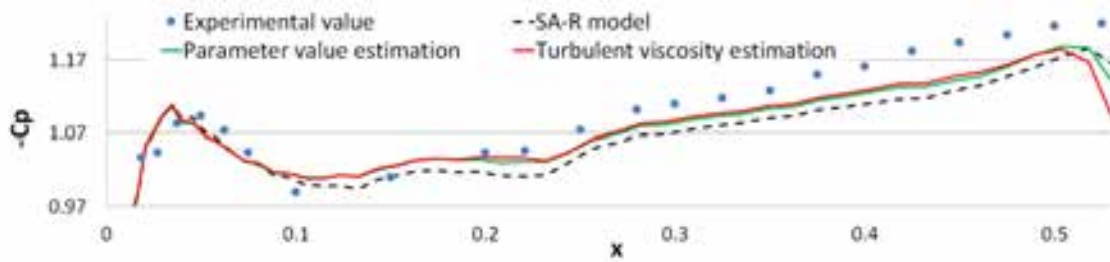
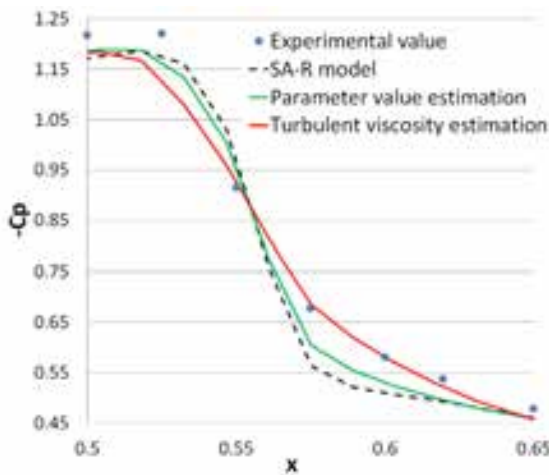


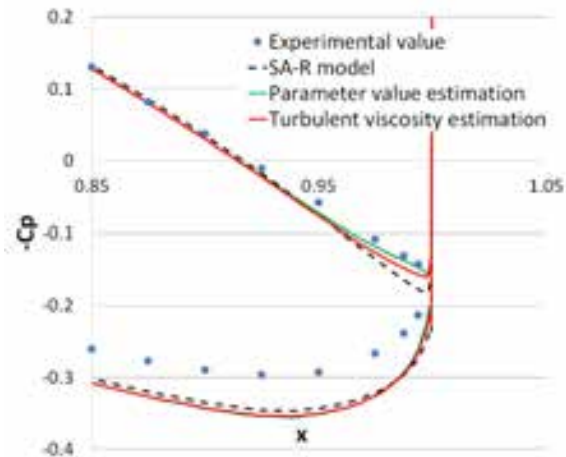
Figure 3. Computed pressure coefficients and experimental values



(a) on upper surface before shock location



(b) at shock-boundary layer interaction



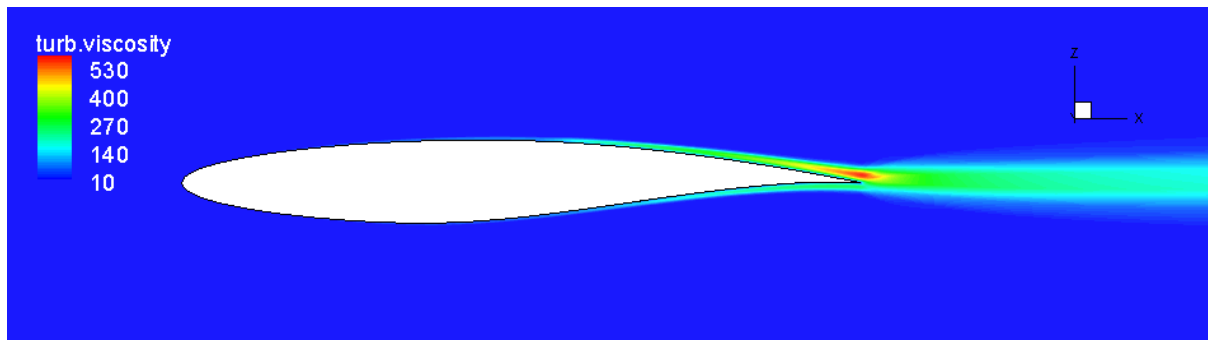
(c) at trailing edge

Figure 4. Computed pressure coefficients and experimental values (Enlarged view)

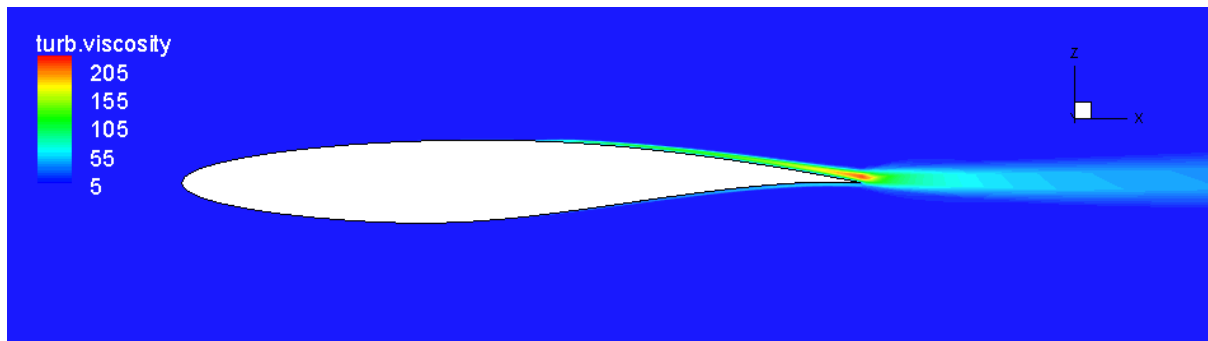
Next, the computed flow of each are compared. The experimental pressure coefficient at the shock-boundary layer interaction suggests that the separated flow occurs. To investigate the computed flow of each in detail, firstly, the computed turbulent viscosity of each are compared.

Figure 5 shows the turbulent viscosity computed with the SA-R model using the original parameter values, that computed with the SA-R model using the adjusted parameter values, and that computed with the ensemble Kalman filter. The computed turbulent viscosity with the ensemble Kalman filter shows:

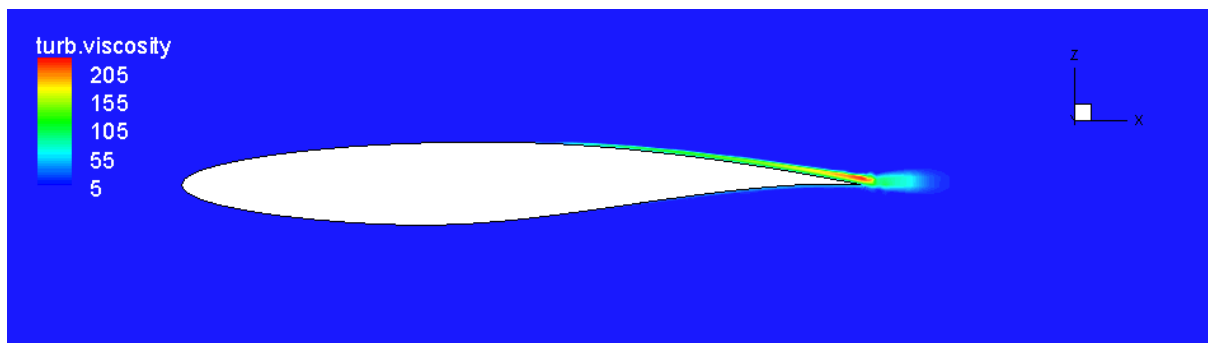
1. Lower turbulent viscosity on the airfoil than that with the SA-R model using the original parameter values.
2. Lowest turbulent viscosity at the wake region of three



(a) SA-R model using original parameter values



(b) SA-R model using adjusted parameter values

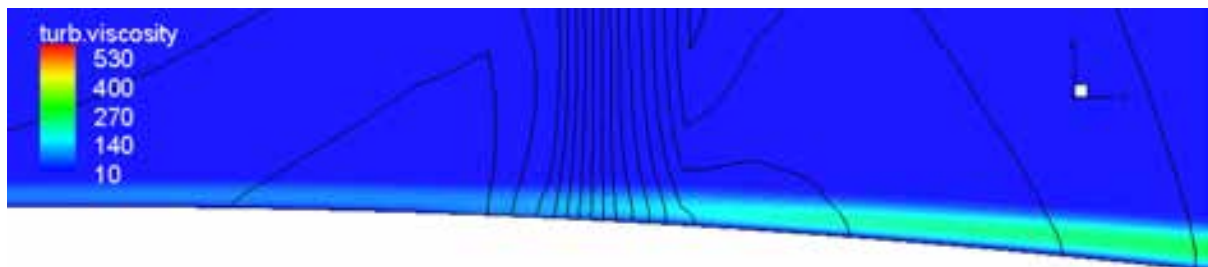


(c) Ensemble Kalman filter

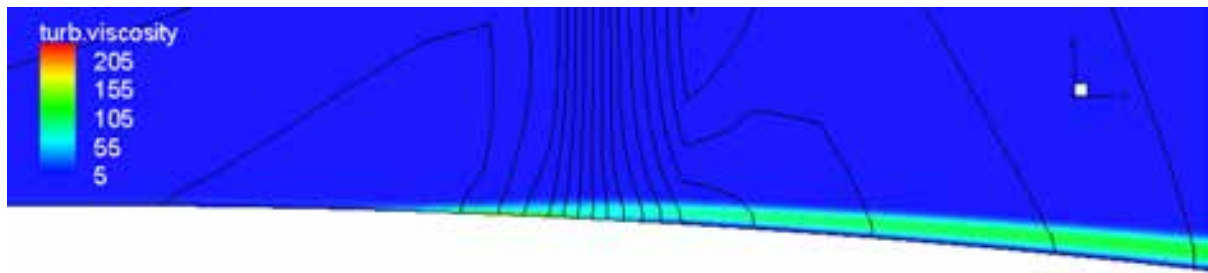
Figure 5. Computed turbulent viscosity

In Fig. 6, the computed turbulent viscosities around the shock location of each are compared. In Fig. 6, the line shows the computed pressure coefficient of each. Each figure shows the following:

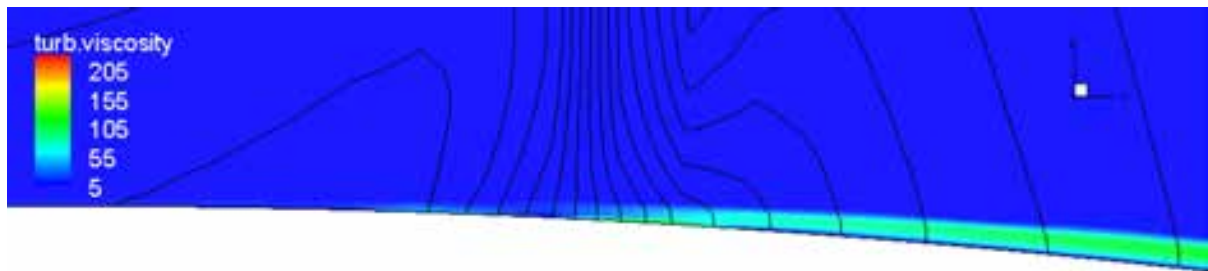
1. The SA-R model using the original parameter values predicts an increase in turbulent viscosity from before the shock location, and the turbulent viscosity before the shock location increases more at the shock location.
2. The SA-R model using the adjusted parameter values predicts an increase in the turbulent viscosity from near the front of the shock location.
3. The ensemble Kalman filter estimates an increase in the turbulent viscosity at the front of the shock location and from the inside of the shock location.



(a) SA-R model using original parameter values



(b) SA-R model using adjusted parameter values



(c) Ensemble Kalman filter

Figure 6. Computed turbulent viscosity around the shock location

Next, the horizontal velocity components of each are compared in Fig. 8. The comparisons are conducted at (a) $x = 0.54$, (b) $x = 0.56$, (c) $x = 0.58$, (e) $x = 0.60$, and (e) $x = 0.62$ on the upper surface as shown in Fig. 7. The experimental pressure distribution indicates that separated flow occurs around the region.

In Fig. 8, the vertical axis shows the vertical distance above the airfoil and the horizontal axis shows the horizontal velocity component. In Fig. 8, the black dotted line shows the computed horizontal velocity component with the turbulent viscosity of the SA-R model using the original parameter values (SA-R model), the green line shows that with the turbulent viscosity of the SA-R model using the adjusted parameter values (Parameter value estimation), and the red line shows that with the turbulent viscosity of the ensemble Kalman filter (Turbulent viscosity estimation).

Each figure shows the following:

1. The computed horizontal velocity component with the turbulent viscosity of the SA-R model using the original parameter values differs from the distribution of separated flow at each location.
2. The computed horizontal velocity component with the turbulent viscosity of the SA-R model using the adjusted parameter values is close to the distribution of separated flow at (c) $x = 0.58$, (d) $x = 0.60$, and (e) $x = 0.62$; however, these are not the distribution of separated flow.
3. The computed horizontal velocity component with the turbulent viscosity of the ensemble Kalman filter is the distribution of separated flow at (b) $x = 0.56$, (c) $x = 0.58$, (d) $x = 0.60$, and (e) $x = 0.62$.

As the experimental pressure coefficient at the shock-boundary layer interaction suggests, the separate flow occurs in the flow computed with “Turbulent viscosity estimation.” This result indicates that the turbulent viscosity estimated by the ensemble Kalman filter was appropriate for computation at the shock-boundary interaction.

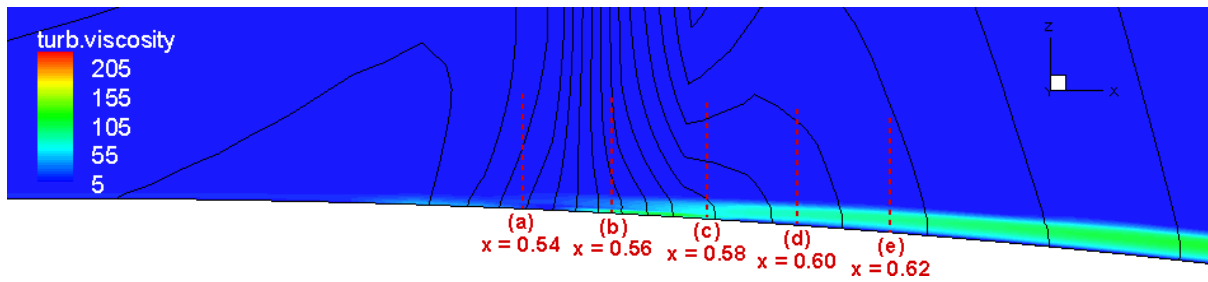


Figure 7. Locations for comparison of horizontal velocity components

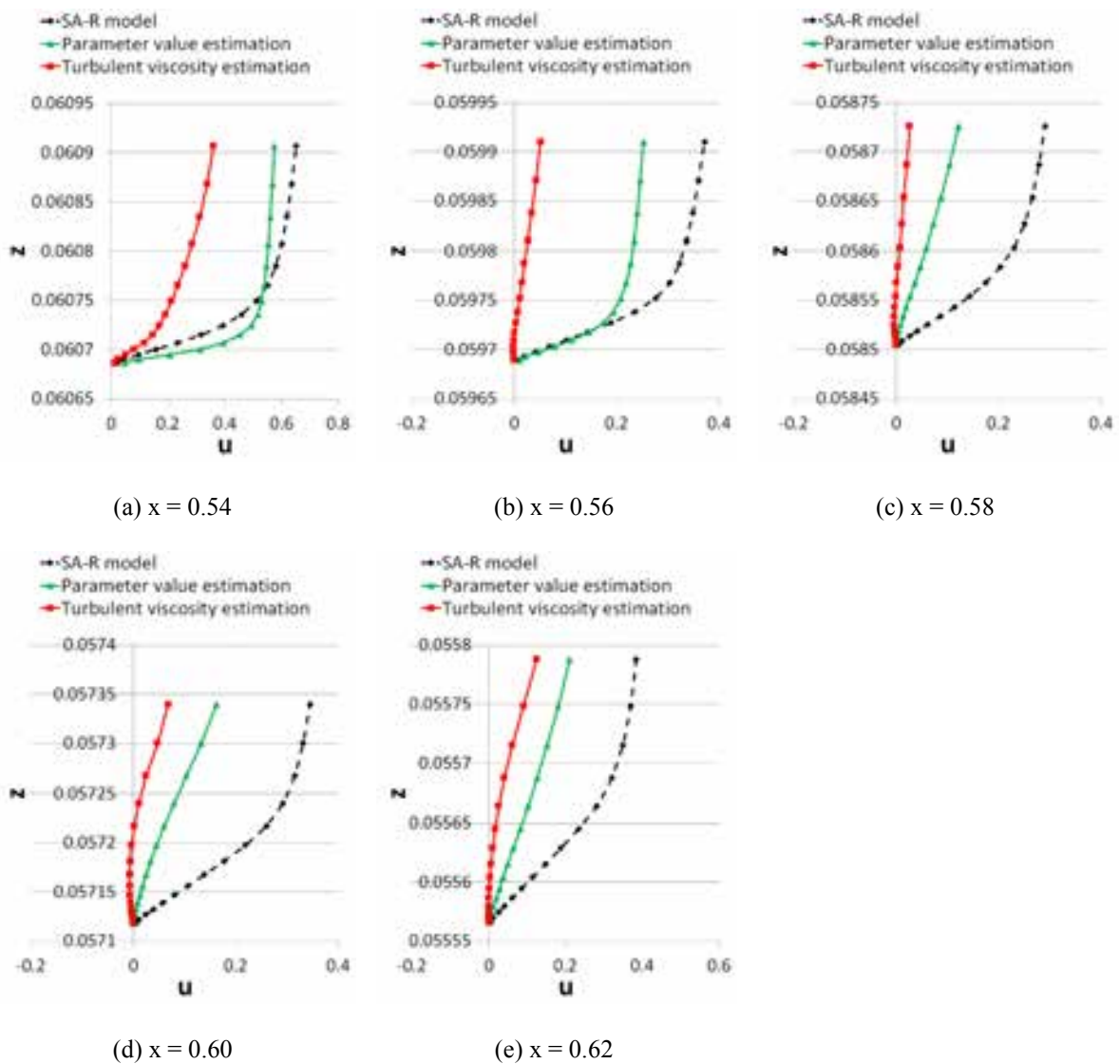


Figure 8. Distributions of horizontal velocity component

Conclusion

In this study, the turbulent viscosity in the flow field around the RAE2822 airfoil was estimated based on the experimental pressure values on the airfoil without a turbulence model. The ensemble Kalman filter, a data assimilation method, was employed to estimate the turbulent viscosity. The initial distribution of each ensemble member that is required in the process of the ensemble Kalman filter, was determined by computation with the Spalart–Allmaras turbulence model (SA-R). In the computation for the initial distribution of each ensemble member, the different parameter values of the SA-R model were assigned to each ensemble member. The turbulence model was used only to determine the initial distribution of each ensemble member. After estimation of the state variables by the ensemble Kalman filter, the estimated state variables other than turbulent viscosity—i.e., density, velocity components, and pressure—were re-computed by the computational schemes alone so that the state variables satisfied the computational schemes.

The estimated turbulent viscosity increased at the front of the shock location and from the inside of the shock location. Compared to the computed turbulent viscosity with the SA-R turbulence model using the original parameter values and the adjusted parameter values, the turbulent viscosity estimated by the ensemble Kalman filter showed (1) lower turbulent viscosity on the upper surface than that with the SA-R model using the original parameter values, and (2) the lowest turbulent viscosity at the wake region of three.

Computation with the estimated turbulent viscosity was able to predict (1) the pressure coefficients that agrees with the experimental pressure coefficients at the shock-boundary interaction, and (2) the separated flow at the shock-boundary interaction. These observations indicated that the estimated turbulent viscosity was appropriate for computation at the shock-boundary interaction and the ensemble Kalman filter was able to be used for estimation based on the experimental pressure distribution on the airfoil without a turbulence model.

These observations suggest that the computation can predict the proper flow field when the proper turbulent viscosity is given.

On the other hand, the present results still show the disagreement with the experiment on the upper surface of the airfoil and at the trailing edge. Although the disagreement might be caused by not the turbulent viscosity but other factors such as two dimensional calculation, this is an issue. Further studies are required to investigate and resolve this issue.

When this issue is resolved and some kind of physical quantity over the entire flow region become available, it will be possible to perform computation without a turbulence model, and the computation can predict the flow field more precisely than either EFD or CFD alone. This will be one form of EFD/CFD.

Appendix

Table 2 shows the computed aerodynamic coefficients with the turbulent viscosity of the SA-R model using the original parameter values (SA-R model), those with the turbulent viscosity of the SA-R model using the adjusted parameter values (Parameter value estimation), and those with the turbulent viscosity of the ensemble Kalman filter (Turbulent viscosity estimation). We do not know which of the computed aerodynamic coefficients are reliable because we do not have the experimental aerodynamic coefficients.

Table 2. Comparison of computed aerodynamic coefficients

| Aerodynamic coefficient | SA-R model | Parameter value estimation | Turbulent viscosity estimation |
|-------------------------|------------|----------------------------|--------------------------------|
| C_D | 0.01338 | 0.01126 | 0.01117 |
| C_L | 0.74098 | 0.74840 | 0.75139 |
| C_m (0.25c) | -0.10139 | -0.10294 | -0.10319 |

References

- [1] S. Watanabe, S. Kuchi-ishi, T. Aoyama.: A Prototype System Towards EFD/CFD Integration: Digital/Analog-Hybrid Wind Tunnel. 27th International Congress of the Aeronautical Sciences, 2010.
- [2] P. R. Spalart and S. R. Allmaras.: A One-Equation Turbulence Model for Aerodynamic Flows. *Recherche Aerospaciale*, No. 1, pp. 5-21, 1994.
- [3] F. R. Menter.: Two-Equation Eddy-Viscosity Turbulence Models for Engineering Applications. *AIAA Journal*, Vol. 32, No. 8, pp. 1598-1605, 1994.
- [4] H. Kato, et al.: Adaptive Simulation of Turbulence Flow by using Data Assimilation. *Journal of Japan Society of Fluid Mechanics*, Vol. 31, No. 2, pp. 165-173, 2012. (in Japanese)
- [5] H. Kato and S. Obayashi.: Approach for Uncertainty of Turbulence Modeling Based on Data Assimilation Technique. *Computers & Fluids Special Issue: Future of CFD*. (submitted for publication)
- [6] H. Kato and S. Obayashi.: Optimization of a Turbulence Model by using Data Assimilation. European Congress on Computational Methods in Applied Sciences and Engineering (ECCOMAS 2012), 2012.
- [7] NPARC Alliance Validation Archive: <http://www.grc.nasa.gov/WWW/wind/valid/raetaf/raetaf05/raetaf05.html>.
- [8] G. Evensen.: Sequential data assimilation with a nonlinear quasi-geostrophic model using Monte Carlo methods to forecast error statistics. *Journal of Geophysical Research*, Vol. 99(C5), pp. 10 143- 10 162, 1994.
- [9] C. Wunsch.: The Ocean Circulation Inverse Problem. Cambridge University Press, 1996.
- [10] G. Evensen.: The ensemble Kalman filter: Theoretical formulation and practical implementation. *Ocean Dynamics*, Vol. 53, pp. 343-367, 2003.
- [11] G. Evensen.: Data Assimilation. *The Ensemble Kalman Filter (2nd ed.)*, Springer-Verlag, 2009.
- [12] G. Evensen.: The ensemble Kalman filter for combined state and parameter estimation. *IEEE Control Systems Magazine*, Vol. 29, No. 3, pp. 83-104, 2009.
- [13] A. Hashimoto, K. Murakami, T. Aoyama, K. Ishiko.: Toward the Fastest Unstructured CFD Code 'FaSTAR'. 50th AIAA Aerospace Sciences Meeting including the New Horizons Forum and Aerospace Exposition, 2012.
- [14] NPARC Alliance CFD Validation Archive: <http://www.grc.nasa.gov/WWW/wind/valid/raetaf/raetaf05/cp.exp.gen>.
- [15] M. D. McKay, R. J. Beckman, W. J. Conover.: A Comparison of Three Methods for Selecting Values of Input Variables in the Analysis of Output from a Computer Code. *Technometrics*, Vol. 21, No. 2, pp. 239-245, 1979.